

QCD on the 16-cell honeycomb

Sandor D. Katz* and Daniel Nogradi†

*Eotvos Lorand University, Institute of Physics and Astronomy,
Department of Theoretical Physics, Budapest, Hungary*

(Dated: December 12, 2025)

We formulate QCD discretized on the four dimensional 16-cell honeycomb. The advantage is a higher degree of rotational symmetry as compared to a traditional cubic lattice leading to much smaller cut-off effects. We demonstrate in quenched QCD, through both gluonic and fermionic observables, that the scaling properties are indeed superior to the cubic lattice and much larger lattice spacings are sufficient for controlled continuum extrapolations. Chiral and topological properties also show remarkable improvement.

INTRODUCTION

The most successful non-perturbative formulation of QCD uses a four-dimensional Euclidean spacetime lattice. Large-scale state of the art lattice simulations face two major challenges: the chiral and continuum extrapolations, both of which are sensitive to the chosen discretization. To preserve as much of the continuum space-time symmetry as possible, one can base the discretization on regular spacetime tessellations – that is, tilings of Euclidean space by regular polytopes. In two dimensions, three regular tessellations exist (triangular, square, and hexagonal), while in three dimensions only the cubic tessellation is possible. In four dimensions, however, there are again three options: the 16-cell honeycomb, the tesseract honeycomb, and the 24-cell honeycomb.

Large-scale QCD simulations have so far relied exclusively on the cubic lattice defined by the vertices of the tesseract honeycomb. The other two regular four-dimensional tessellations, however, possess larger remnant rotational symmetry. Specifically, the symmetry group of the cubic lattice has 384 elements, whereas the symmetry groups of the vertex sets of both the 16-cell and 24-cell honeycombs contain 1152 elements.

In this work, we investigate lattice QCD formulated on the vertices of the 16-cell honeycomb. Interestingly, this lattice corresponds to the densest sphere packing in four-dimensional Euclidean space: each site has 24 nearest neighbors, equal to the four-dimensional kissing number. We find that cutoff effects are substantially reduced and that lattice spacings lying outside the scaling regime of the cubic formulation fall comfortably within it on this lattice. Furthermore, chiral properties are also superior to the cubic discretization.

The first hints that cut-off effects are much smaller using the 16-cell honeycomb rather than the cubic lattice come from free fields. For instance, the pressure of massless free fermions at finite temperature, if renormalized suitably, has $\mathcal{O}(a^2)$ cut-off effects on a cubic lattice but only $\mathcal{O}(a^4)$ for the 16-cell honeycomb. Beyond free fields, we study the cut-off effects of the topological susceptibility in $SU(3)$ gauge theory and show that even in the interacting case cut-off effects appear to be $\mathcal{O}(a^4)$ only.

Turning to the naive discretization of fermions it should be noted that the 16-cell honeycomb was investigated before [1–7] and the dispersion relation of some of the doublers were shown to break Lorentz invariance. This problem is eliminated, however, by adding a Wilson term to the action which pushes the mass scales of the doublers to the cut-off scale as usual. The physical mode remains massless and its dispersion relation Lorentz invariant, leading to a physical spectrum free from any Lorentz breaking in the continuum. We show, in quenched QCD, that the Dirac spectrum and the topological properties of low modes is quantifiably closer to the continuum than the corresponding quantities on a cubic lattice, at fixed lattice spacing.

It should be noted that the same lattice and its sublattices were also investigated in Higgs models in the context of triviality in the past [8–10]. Exactly because scalar QFT is trivial, the strict continuum limit cannot be addressed of course.

Our work is the first to report on the systematics of the continuum extrapolation of $SU(3)$ gauge theory and the properties of quenched QCD on this lattice of highest possible symmetry in 4 dimensions.

THE 16-CELL HONEYCOMB

The vertex set of the 16-cell honeycomb is known by multiple names: the body-centered cubic or tesseract (BCH or BCT) lattice, or the D_4 , D_4^* , or F_4 lattice. The lattice sites in 4-dimensions can be defined for instance by requiring that all four components are integers and their sum is even, in lattice units (D_4 lattice). Alternatively, one may define it by having a usual 4-dimensional cubic lattice and adding the centers of each hypercube (BCH lattice). Any lattice can be defined by a set of basis vectors and lattice sites are given by integer linear combinations. The set of basis vectors is of course not unique: if these are arranged as columns into a 4×4 matrix e then transformations of the type $e \rightarrow \lambda R e K^{-1}$ are immaterial, where $\lambda \in \mathbb{R}$ non-zero, $R \in O(4)$ and $K \in GL(4, \mathbb{Z})$. Here λ corresponds to an overall rescaling, R to an overall rotation of the basis vectors while K

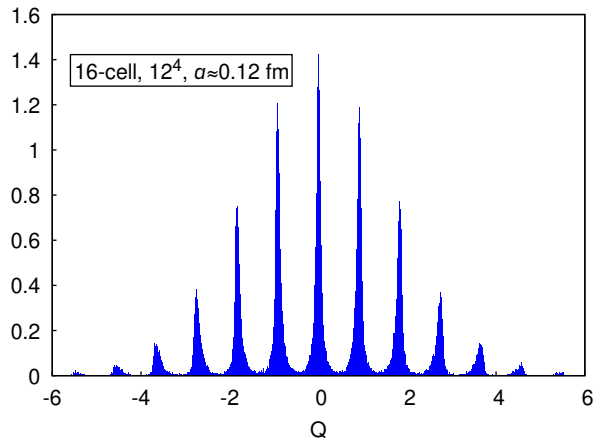


FIG. 1. Distribution of the topological charge on the 16-cell honeycomb. For clarity we do not show the corresponding histogram with the cubic lattice, but as can be expected, the $a = 0.12$ fm lattice spacing is too large for clear peaks in that case.

simply relabels the integers. Two frequently used choices of e basis matrices for the 16-cell honeycomb are the following,

$$\begin{pmatrix} 1 & 0 & 0 & 0 \\ -1 & 1 & 0 & 0 \\ 0 & -1 & 1 & 1 \\ 0 & 0 & -1 & 1 \end{pmatrix} \quad \begin{pmatrix} 1 & 0 & 0 & 1/2 \\ 0 & 1 & 0 & 1/2 \\ 0 & 0 & 1 & 1/2 \\ 0 & 0 & 0 & 1/2 \end{pmatrix}, \quad (1)$$

and depending on context one is more useful than the other. Each lattice site thus has 24 nearest neighbors, 12 of these in the positive and 12 in the negative direction. This enlarged set of nearest neighbors is the main reason for the enlarged rotational symmetry.

Once the lattice becomes finite and (anti)periodic boundary conditions are imposed, the choice of basis will matter, because they will set the directions in which there is (anti)periodicity. At finite temperature this choice clearly matters in the temporal direction. In the present work the second choice in (1) is used in the simulations. We fix the boundary conditions such that they correspond to an orthogonal torus: a periodicity of N_s sites is imposed in the (1000), (0100), (0010) directions while (anti)periodicity of N_t sites is assumed in the (0001) direction. Note that the boundary conditions break the full rotational symmetry but this has little impact on the observed scaling properties, as was also noted in [3].

Using this setup, for a given physical volume and lattice spacing our lattice contains twice as many sites as the cubic one. Since each site has three times as many nearest neighbors, the naive computational cost of the 16-cell discretization is 6 times that of the cubic one.

For more details on numerous aspects of the 16-cell honeycomb see [11].

GLUONS

Gauge links can naturally be defined for each link of the lattice, just as in the cubic case. An elementary closed loop is a triangle, however, and so the basic building block of the gauge action will contain sums over triangles. At each site of the lattice there are 192 oriented triangles emanating from that site, half of them positively oriented and half of them negatively. Since a triangle has 3 corners, in order to avoid over counting, we need to sum over 32 triangles for each site, leading to the $SU(N)$ gauge action,

$$S = \frac{\beta}{2} \sum_x \sum_{i=1}^{32} \left(1 - \frac{1}{N} \text{Re Tr } P_i(x) \right) \quad (2)$$

where $P_i(x)$ is the product of the 3 links in the given triangle. The overall normalization ensures that $\beta = 2N/g_0^2$ with bare coupling g_0 just as with the cubic action.

We report on the continuum limit and scaling property of the topological susceptibility in t_0 units, hence let us define the topological charge from basic triangles and the gradient flow [12] as well. A symmetric definition of the topological charge is adopted akin to the clover-type definition on the cubic lattice. With the 16-cell honeycomb there are 6 basic triangles with a common corner in a given plane. These 6 basic triangles form a hexagon and there are 16 hexagons at a given site. From these 16 hexagons the field strength tensor components can be defined in a symmetric manner, from which the topological charge density as well as the total topological charge follow.

The gradient flow also follows straightforwardly from the action (2), one only needs to take into account the non unit area of a basic triangle. The distribution of the topological charge, evaluated at $t = t_0$ on the 16-cell honeycomb is shown in figure 1 with clear peaks close to integer values already at $a = 0.12$ fm. Here and in the following $\sqrt{8t_0} = 0.47$ fm is used to set the scale.

Once all ingredients are given, figure 2 shows the continuum limit of the topological susceptibility χ in t_0 -units. The volume is kept fixed also in t_0 -units, the bare couplings are tuned to $L/\sqrt{8t_0} = 3$ within 1% accuracy on lattice volumes $6^4, 8^4, 9^4, 10^4, 11^4$ and 12^4 . We used standard local overrelaxation and heatbath updates and generated $\mathcal{O}(50000)$ independent configurations for each lattice. The results are compared to the corresponding ones on a cubic lattice from [13]. While there is clear agreement for the continuum limit, as it should be, the leading cut-off effects are drastically reduced and appear to follow $\mathcal{O}(a^4)$ to high precision. We performed two fits for the continuum extrapolation: one with $\mathcal{O}(a^2)$ and $\mathcal{O}(a^4)$ terms and one with only $\mathcal{O}(a^4)$. The $\chi^2/\text{d.o.f.}$ values are 0.34 and 0.30, respectively and the $\mathcal{O}(a^2)$ coefficient is consistent with zero in the first case. Its 1σ upper bound is an order of magnitude smaller than the

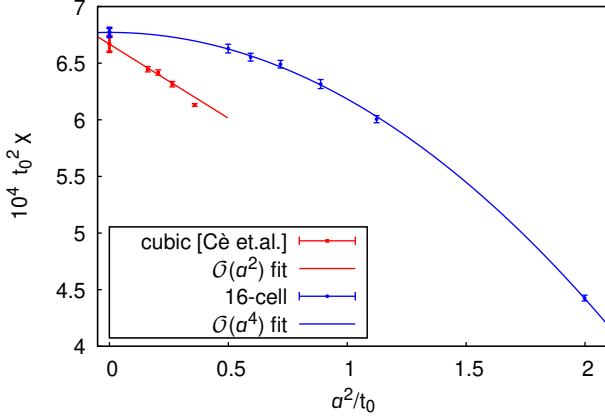


FIG. 2. Continuum limit of the topological susceptibility. Solid lines show the extrapolations; see text for details.

$\mathcal{O}(a^2)$ coefficient on the cubic lattice. Therefore in the plot we show the $\mathcal{O}(a^4)$ fit only. Lattice spacings as large as $a = 0.24$ fm can be used in the fit, which are definitely outside the leading scaling regime of $\mathcal{O}(a^2)$ with a cubic lattice.

QUARKS

Quark fields are defined at each site as usual. The naive discretization of the free massless Dirac operator, summing over all neighbors,

$$D_0 = \frac{1}{6} \sum_{i=1}^{24} \gamma_\mu n_{\mu i} \nabla_i, \quad (3)$$

where $n_{\mu i}$ are the 24 neighbor directions, leads to Lorentz violating doublers [2]. Here the overall factor $1/6$ is dictated by the correct p^2 normalization of $D_0^\dagger D_0$ in momentum space.

Let us add a Wilson term with coefficient r which, just as in the cubic case, pushes the doublers to the cut-off scale leaving a single Lorentz invariant physical massless flavor in the continuum,

$$D = D_0 + a \frac{r}{6} \sum_{i=1}^{24} \nabla_i^* \nabla_i, \quad (4)$$

where again the factor $1/6$ ensures that in momentum space the Wilson term becomes $ar p^2/2$ for small momenta, as usual. Figure 3 shows the free spectrum of the 16-cell honeycomb Wilson-Dirac operator (4) in comparison with the cubic case. A striking observation is obvious: the spectrum appears to be much closer to a chirally invariant Ginsparg-Wilson-like circle than Wilson fermions on a cubic lattice, which is very promising.

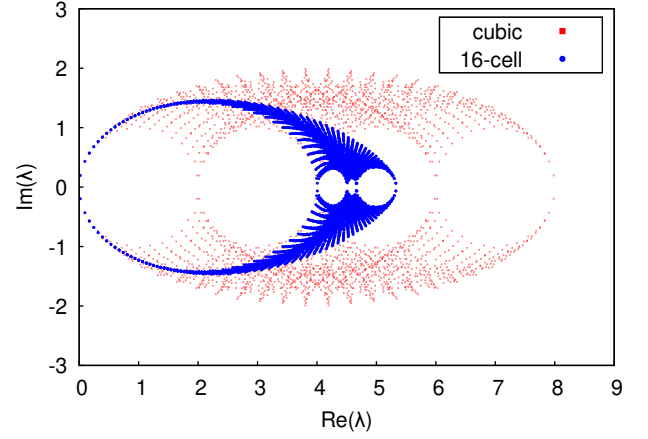


FIG. 3. Comparison of the free Wilson-Dirac spectra on lattice volumes 16^4 .

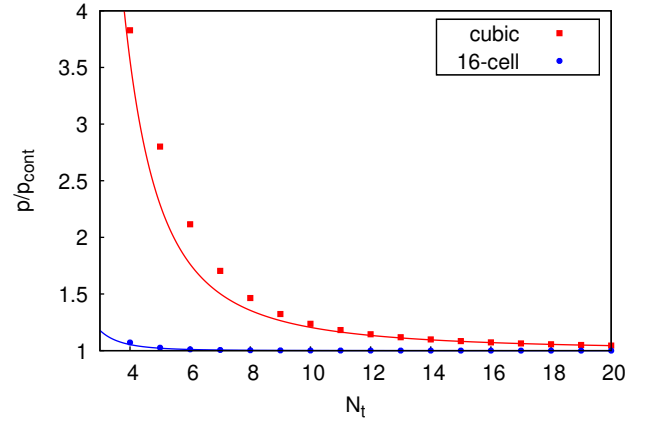


FIG. 4. The pressure as a function of N_t normalized by the continuum values. The solid lines show the analytic $\mathcal{O}(1/N_t^2)$ and $\mathcal{O}(1/N_t^4)$ scalings of the two discretizations given by eqn (5).

Another quantity, which in the free case also shows promising improved scaling, is the pressure at finite temperature. Let us subtract the zero temperature pressure, as usual, in order to have no additive divergences, and study $\mathcal{O} = (p(T) - p(0))/T^4$. Corrections to the continuum value in infinite spatial volume can be straightforwardly computed as a series in $1/N_t^2$, and we obtain,

$$\begin{aligned} \mathcal{O}_{cubic} &= \frac{7\pi^2}{720} \left(1 + \frac{248}{147} \frac{\pi^2}{N_t^2} + \frac{635}{147} \frac{\pi^4}{N_t^4} \dots \right) \\ \mathcal{O}_{16-cell} &= \frac{7\pi^2}{720} \left(1 + \frac{127}{980} \frac{\pi^4}{N_t^4} + \frac{73}{4158} \frac{\pi^6}{N_t^6} + \dots \right). \end{aligned} \quad (5)$$

The leading corrections in the 16-cell honeycomb case are $\mathcal{O}(a^4)$ as opposed to $\mathcal{O}(a^2)$ in the cubic case, a major improvement. Figure 4 shows the scaling behavior at finite N_t , in full agreement with the asymptotic forms (5). At $N_t = 4$, for instance, the correction to the con-

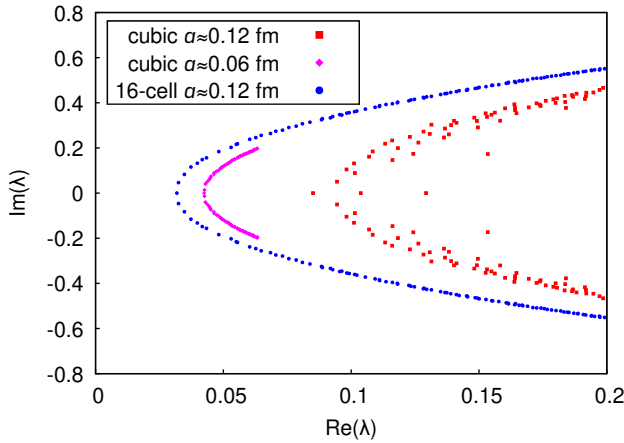


FIG. 5. Comparison of quenched Wilson-Dirac spectra on 12^4 lattice volumes. For the cubic case we also show results on a finer, 24^4 lattice. Each spectrum corresponds to a single configuration.

tinuum is 7% and 283% on the 16-cell and cubic lattices, respectively, while at $N_t = 6$ these are 1% and 110%, respectively. In order to replicate on the cubic lattice the rather small 7% and 1% corrections of the 16-cell lattice at $N_t = 4$ and $N_t = 6$, one would need $N_t = 16$ and $N_t = 40$.

The fact that the leading correction is $\mathcal{O}(a^4)$ can be understood from the form of the corrections to the dispersion relation. It is a straightforward expansion in the lattice spacing to obtain

$$D^\dagger D = p^2 - \frac{1}{6}a^2 p^4 + \mathcal{O}(a^4) \quad (6)$$

i.e. at order $\mathcal{O}(a^2)$ the correction is still Lorentz invariant, the first order where this does not hold is $\mathcal{O}(a^4)$. With a cubic lattice, already at order $\mathcal{O}(a^2)$ we encounter Lorentz breaking terms. As a consequence, on a 16-cell honeycomb the dispersion relation becomes, in Minkowski signature, $E = |\mathbf{p}| + \mathcal{O}(a^4)$, leading to the absence of the $\mathcal{O}(a^2)$ correction in the pressure.

Let us turn to the interacting case, inserting gauge links into (4), and implementing tree-level clover improvement [14] as well as stout smearing [15]. The field strength tensor for clover improvement is obtained at each site from the 16 hexagons, similarly to the gradient flow. Six steps of stout smearing are applied with smearing parameter $\varrho = 0.05$. In this first work we only study quenched QCD and our focus will be the comparison with the Wilson-Dirac operator on a cubic lattice using the same improvement, i.e. tree-level clover and stout smearing using the same parameters. In order to have meaningful comparisons the lattice spacings are tuned to $a \approx 0.12$ fm for both discretizations. We determined the lowest 300 eigenvalues of the Wilson-Dirac operator on 1215 quenched configurations generated on 12^4 lattices

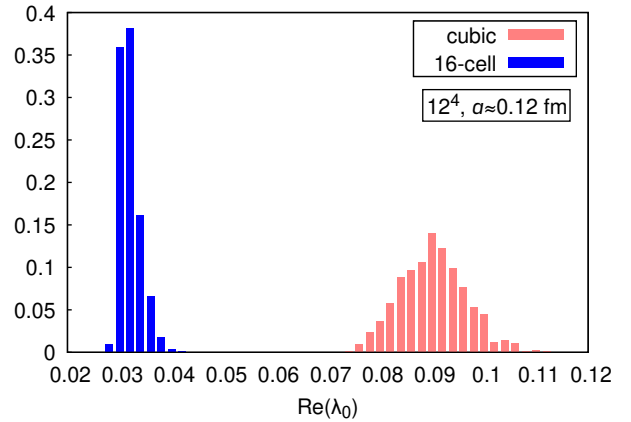


FIG. 6. Comparison of the distribution of the lowest Wilson-Dirac eigenvalue.

with both discretizations. In addition, we computed the lowest 100 eigenvalues on a single quenched 24^4 configuration with $a \approx 0.06$ fm

The low-lying quenched Wilson-Dirac spectra evaluated on single configurations are shown in figure 5. Two things are immediately clear, first, at the same lattice spacing the additive mass renormalization will be much smaller on the 16-cell honeycomb and second, the width of the distribution of the real part of the lowest eigenvalues is also much smaller. The first property results in improved chiral properties while the second means that smaller quark masses can be simulated at a given lattice spacing, something with important practical consequences towards the chiral limit. For comparison we also show results on the cubic lattice at half the lattice spacing and twice the linear lattice size, i.e. the same physical volume, which still results in larger additive mass renormalization. For a more detailed look the distribution of the real part of the lowest eigenvalue is shown in figure 6. We observe a factor of three improvement both for the mean and for the width of the distribution by using the 16-cell honeycomb.

The Wilson-Dirac operator has no exact chiral symmetry, nevertheless the low-lying real eigenvalues carry important topological information. One may count the number of real low-lying eigenvalues with non-zero chirality (n_+ and n_- for positive and negative chiralities, respectively)[16] and thus define $Q_{\text{Dirac}} = n_+ - n_-$ as a topological charge. We compare this to Q_{flow} defined using the gradient flow at $t = t_0$ as in the calculation of the topological susceptibility. These two quantities are of course not necessarily the same, but towards the continuum limit they are expected to approach each other. The distribution of the difference $Q_{\text{Dirac}} - Q_{\text{flow}}$ is shown in figure 7. The conclusion is the same as for the quenched Wilson-Dirac spectrum: at the same lattice spacing the 16-cell honeycomb appears to be much closer to the con-

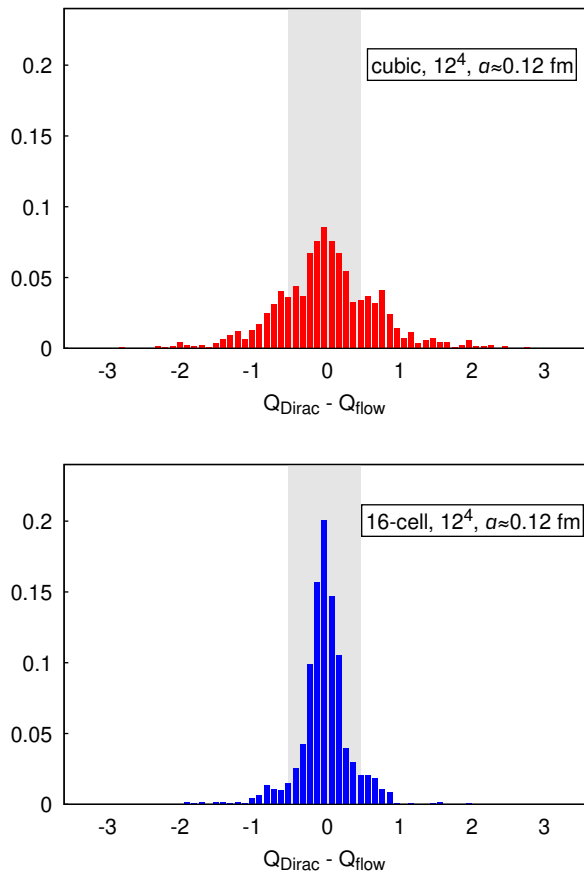


FIG. 7. The distribution of the difference of fermionic and gluonic definitions of the topological charge. Top: cubic lattice, bottom: 16-cell honeycomb. The gray bands correspond to the range $[-0.5:0.5]$ where a rounding of Q_{flow} would match Q_{Dirac} .

tinuum, with practically no configuration showing a difference larger than 1. The index theorem is quite accurately realized already at a lattice spacing $a \approx 0.12$ fm.

Another measure of the topological character of low-lying real modes is how close or far their chirality is from ± 1 . With chirally symmetric fermion discretizations the zero modes have definite chirality. With Wilson-Dirac fermions this does not hold but the distribution of the chiralities is a good measure of their topological nature. This is shown in figure 8. The difference between the cubic lattice and the 16-cell honeycomb is again striking.

Summarizing our findings, it is clear that at comparable lattice spacings the properties of the Wilson-Dirac operator on the 16-cell honeycomb are much closer to the continuum than on a cubic lattice. Even though there is a factor 6 increase in computational cost, this is more than compensated by larger lattice spacings being sufficient for fixed “continuum-like” properties, i.e. larger lattice spacings and smaller lattice volumes are sufficient for con-

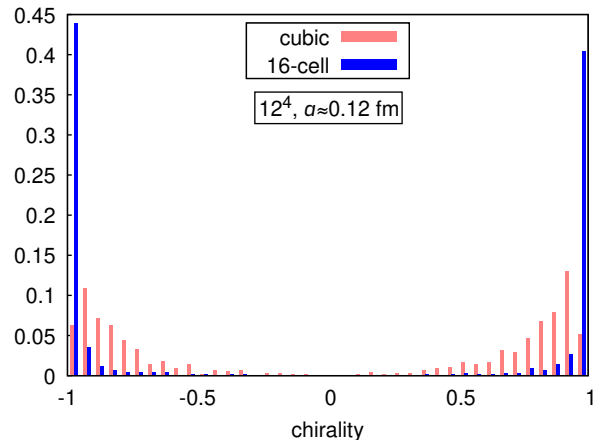


FIG. 8. Comparison of distributions of chiralities of low-lying real Wilson-Dirac eigenvalues.

trolled and reliable continuum extrapolations. Furthermore, the smaller additive mass renormalization allows for lower quark masses to be simulated at a given lattice spacing.

CONCLUSION AND OUTLOOK

We have investigated lattice QCD discretized on the vertex set of the 16-cell honeycomb, instead of the traditional cubic one. In several observables $\mathcal{O}(a^4)$ leading scaling corrections are observed, leading to a much larger range of lattice spacings from which reliable continuum extrapolations can be performed.

Our discussion involved gluons and quarks but so far only in the quenched approximation. The improved chiral and topological properties of the Wilson-Dirac operator relative to the cubic case indicates that larger lattice spacings and consequently smaller lattice volumes can be used for controlled continuum extrapolations. Furthermore, at a fixed lattice spacing smaller quark masses can be simulated. Both of these properties, better chiral properties and better continuum scaling lead to significant advantages when considering computational costs. Our results both for gluonic and fermionic observables suggest that on the 16-cell honeycomb about twice larger lattice spacings can be used than on the cubic lattice with the same discretization effects. This may lead to as large as an order of magnitude reduction in total computational costs.

We plan to exploit these features further in fully dynamical QCD simulations in future publications.

ACKNOWLEDGMENTS

We are grateful for G. Endrődi, M. Giordano, T.G. Kovács and A. Pásztor for useful discussions. This work was supported by NKFIH grants No. TKP2021-NKTA-64, NKKP Excellence No. 151482 and K-147396. All computations were performed on the local GPU cluster at Eotvos University.

* katz@bodri.elte.hu

† nogradi@bodri.elte.hu

- [1] W. Celmaster, Phys. Rev. D **26**, 2955 (1982)
- [2] W. Celmaster and F. Krausz, Phys. Rev. D **28**, 1527 (1983)
- [3] W. Celmaster, Phys. Rev. D **28**, 2076 (1983)
- [4] W. Celmaster, Phys. Rev. Lett. **52**, 403 (1984)
- [5] W. Celmaster and K. J. M. Moriarty, Comput. Phys. Commun. **34**, 415-425 (1985)
- [6] W. Celmaster, E. Kovacs, F. Green and R. Gupta, Phys. Rev. D **33**, 3022 (1986)
- [7] W. Celmaster and K. J. M. Moriarty, Phys. Rev. D **33**, 3718 (1986)
- [8] H. Neuberger, Phys. Lett. B **199**, 536-540 (1987)
- [9] G. Bhanot, K. Bitar, U. M. Heller and H. Neuberger, Nucl. Phys. B **343**, 467-506 (1990)
- [10] G. Bhanot, K. Bitar, U. M. Heller and H. Neuberger, Nucl. Phys. B **353**, 551-564 (1991) [erratum: Nucl. Phys. B **375**, 503-503 (1992)]
- [11] J. H. Conway and N. J. A. Sloane, Sphere Packings, Lattices and Groups, Grundlehren der mathematischen Wissenschaften, vol 290, Springer 1999
- [12] M. Lüscher, JHEP **1008**, 071 (2010) Erratum: [JHEP **1403**, 092 (2014)] [arXiv:1006.4518 [hep-lat]].
- [13] M. Cè, C. Consonni, G. P. Engel and L. Giusti, Phys. Rev. D **92**, no.7, 074502 (2015) [arXiv:1506.06052 [hep-lat]].
- [14] B. Sheikholeslami and R. Wohlert, Nucl. Phys. B **259**, 572 (1985)
- [15] C. Morningstar and M. J. Peardon, Phys. Rev. D **69**, 054501 (2004) [hep-lat/0311018].
- [16] P. Hernandez, Nucl. Phys. B **536**, 345-362 (1998) [arXiv:hep-lat/9801035 [hep-lat]].